

Dalton Transactions

Accepted Manuscript



This is an *Accepted Manuscript*, which has been through the Royal Society of Chemistry peer review process and has been accepted for publication.

Accepted Manuscripts are published online shortly after acceptance, before technical editing, formatting and proof reading. Using this free service, authors can make their results available to the community, in citable form, before we publish the edited article. We will replace this *Accepted Manuscript* with the edited and formatted *Advance Article* as soon as it is available.

You can find more information about *Accepted Manuscripts* in the [Information for Authors](#).

Please note that technical editing may introduce minor changes to the text and/or graphics, which may alter content. The journal's standard [Terms & Conditions](#) and the [Ethical guidelines](#) still apply. In no event shall the Royal Society of Chemistry be held responsible for any errors or omissions in this *Accepted Manuscript* or any consequences arising from the use of any information it contains.

One-step fabrication of functionalized magnetic adsorbents with large surface area and their adsorption for dye and heavy metal ions

Jianzhi Wang, Guanghui Zhao, Yanfeng Li*, Hao Zhu, Xiaomen Peng, Xian Gao

State Key Laboratory of Applied Organic Chemistry, Key Laboratory of Nonferrous Metal Chemistry and Resources Utilization of Gansu Province, College of Chemistry and Chemical Engineering, Institute of Biochemical Engineering & Environmental Technology, Lanzhou University, Lanzhou 730000, China

Abstract: Functionalized magnetic adsorbents (FMAs) were synthesized by a facile and surfactant-free one-pot solvothermal approach, using iron (III) chloride hexahydrate as precursor, ethylene glycol as reducing agent, ammonium acetate, as well as EDTA-2Na as electrostatic stabilization agent. The self-assembly process of functionalized magnetic adsorbents has been investigated and a plausible mechanism is proposed. The resulting functionalized magnetic adsorbents held relatively high specific surface areas ($71.6 \text{ m}^2/\text{g}$), excellent magnetic property and rich functional groups (carboxyl group, hydroxyl group and hydrophobic group). Meanwhile, the resulting FMAs were employed in the adsorption for dye and heavy metal ions from aqueous solution. Herein, we took two types of typical pollutants, dye (methylene blue (MB) and malachite green (MG) and toxic heavy metal ions (Cr(VI) and Pb(II)) as the example of organic and inorganic pollutant in water environment. The excellent intrinsic properties lead to a stronger

* Corresponding author. Tel. +86-931-8912528, E-mail: liyf@lzu.edu.cn

adsorption ability of FMAs than the solid Fe_3O_4 adsorbent for MB, MG, Cr(VI) and Pb(II). Especially, the simultaneous adsorption of the functionalized flower-like magnetic adsorbents for MG and Pb(II) was also determined in the binary system. Finally, it was demonstrated that resulting flower-like magnetic adsorbents are expected to be good candidate of adsorbent for water treatment.

Keywords: *functionalized magnetic adsorbent; large surface area; Adsorption; dye; heavy metal ions.*

1. Introduction

Water pollution has been a very big issue in recent years due to the improper treatment of living and industrial wastes before they are drained into river. Various pollutants from industry are found to have an adverse impact on public health and social economy, especially for the water pollution caused by heavy metal ions and dyes.¹ Thus, there is an urgent demand for the removal of such pollutants. To purify the contaminated water, various methods have been used to remove metal ions and dyes from wastewater, such as chemical precipitation, membrane filtration, photodegradation, ion exchange and adsorption, and so on. Among these methods, adsorption is the most versatile and effective one because of its ease of operation, regeneration and low cost, in which many effective adsorbents have been developed by using activated carbon, zeolites, chitosan, fly ash, graphene, polymeric materials and clays.¹⁻⁴ However, these adsorbents usually exhibit high capacity only towards a certain type of pollutants. Therefore, it is a challenge to develop novel methods for the preparation of a broad spectrum adsorbent with high adsorption capacity for water purification.

Recently, different morphologies of micro/nano-structures with large surface areas and rich functional groups were used as the adsorbents for the adsorption of inorganic and organic pollutants. Among various morphologies, the fabrication of three-dimensional (3D) hierarchical inorganic micro/nano-materials by using nanoparticles (0D), nanorods (1D), and nanoplates (2D) as building blocks, have attracted considerable attention because of their unique properties and potential applications in catalysis, energy conversion and storage, environmental abatement, and sensors. To date, a number of highly complex hierarchical micro/nano-architectures have been reported.⁵⁻⁹ However, from a practical point of view; such adsorbents would encounter problems in particles separation and recycling. Taking this into account, micro/nanometre-sized hierarchical metal oxides with their permeable shells, high surface area are one of the most suitable candidates for wastewater treatment compared to their bulk counterparts.^{10,11} Recent reports have demonstrated that hierarchical flower-like Fe_3O_4 and $\gamma\text{-Fe}_2\text{O}_3$ microstructures have been successfully synthesized by the template methods and the hydrothermal/solvothermal approaches.^{6,12,13} However, the lack of surface functional groups of these materials limits their application for pollutant removal. Inspired by their work, it is interesting to prepare and assemble functionalized flower-like magnetic adsorbents with relatively high specific surface areas, excellent magnetic property and rich functional group for the treatment of wastewater.

Over past decades, there have been few reports about the synthesis of functionalized flower-like magnetic adsorbents (~150 nm) with large surface area because of the lack of

new breakthroughs in the synthesis method. In this paper, a one-step, and environment-friendly solvothermal method for the synthesis of functionalized flower-like magnetic adsorbent without the addition of any surfactant is reported. The self-assembly process of the FMAs has been investigated and a possible formation mechanism is proposed. Furthermore, the magnetic property, high specific surface area ($71.6 \text{ m}^2/\text{g}$), large saturation magnetization (44.41 emu/g), and rich functional group (carboxyl group, hydroxyl group and hydrophobic group) are all determined for the obtained FMAs. Inspired by the novel assembled submicron structures and their wonderful intrinsic properties, the as-obtained FMAs revealed an excellent ability to adsorb pollutants when used as adsorbent for the adsorption of dyes and heavy metal ions.

2 Experimental

2.1 Chemicals

Tetraethoxysilane (TEOS) and n-octadecyltrimethoxysilane (C18TMS) were purchased from Sigma-Aldrich; other chemicals and solvents were all of analytical grade and obtained from Tianjing Chemical Reagent Company (China).

2.2 Synthesis of the flower-like magnetic adsorbents

The FMAs were prepared by a modified conventional solvothermal method.¹⁴ In a typical synthesis, 0.8 g of $\text{FeCl}_3 \cdot 6\text{H}_2\text{O}$ was firstly dissolved into 40 mL of ethylene glycol, and then 2.0 g of ammonium acetate (NH_4Ac) and 0.3 g of ethylenediaminetetraacetic acid disodium salt (EDTA-2Na) were added with constant stirring for 30 min. After that, a mixture of 0.225 mL TEOS and 0.05 mL C18TMS were ultrasonically dispersed in the

resulting dispersion for 1 h. The mixture was sealed in a teflon-lined stainless steel autoclave (50 mL capacity) and maintained at 200 °C for 10 h. After the system was cooled down to room temperature naturally, the resulting product was washed with ethanol and deionized water in sequence, and dried in vacuum at 60 °C for 24 h.

2.3 Characterization

The products were analyzed by X-ray diffraction (XRD), in a 2θ range from 10° to 90°, using Cu-K α radiation (Rigaku D/MAX-2400 diffractometer). The morphology of the prepared FMAs were studied by scanning electron microscopy (SEM, Hitachi S-4800) and transmission electron microscopy (TEM, FEI Tecnai G20), high angle annular dark field and scanning transmission electron microscopy (HAADF-STEM) (Philips X'pert Pro MPD, Netherlands). Fourier transform infrared spectroscopy (FT-IR) was performed on a Nicolet Nexus 670 FTIR spectrometer using KBr pellet technology. Thermogravimetric/differential thermal analysis (TG-DTA) was conducted with a Netzsch STA 409C thermoanalyzer instrument. Magnetic measurements were performed with a vibrating sample magnetometer (LAKESHORE-7304, USA) at room temperature. The Brunauer-Emmett-Teller (BET) specific surface areas and pore size distributions of the resulting products were measured with a Micromeritics ASAP 2010M instrument. The filtrates were analyzed by recording variations in the maximum absorption band using a lengguang (china) UV-7225 UV-vis spectrophotometer.

2.4 Adsorption studies

The adsorption kinetics and adsorption isotherms were investigated by batch

experiments. For batch tests, a given amount of adsorbent (16 mg) was added into aqueous solution (8 mL) at a known initial concentration, constant temperature of 30 °C and constant rate 120 rpm in a shaking-table under dark environment. After magnetic separation using a permanent magnet, the solution was removed out and the concentration was measured with a UV-vis spectrophotometer.

The adsorption capacity at equilibrium (q_e , mg/g), and the percentage removal (*Removal*, %) can be calculated by the following equations:

$$q_e = \frac{(C_o - C_e)V}{m} \quad (1)$$

$$\text{Removal}(\%) = \frac{C_o - C_e}{C_o} \times 100\% \quad (2)$$

Where q_e is the adsorption capacity (mg/g), C_o (mg/L) and C_e (mg/L) are the initial and equilibrated concentrations, respectively, V (L) is the volume of solution added, and m (g) is the mass of the adsorbent.

3 Results and discussion

3.1 Characterization of magnetic adsorbents

The crystalline structures of the synthesized product were first analyzed by a powder X-ray diffraction (XRD) technique. Fig. S1 gives the XRD pattern of the pure Fe₃O₄ spheres¹⁴ and the FMAs. All the diffraction peaks of both particles were indexed to typical XRD patterns of Fe₃O₄ (JCPDS 75&1609), indicating the formation of magnetite products. The sharp and strong diffraction peaks also confirm the solid crystallization of both particles.

The compositions of FMAs were studied by Fourier transform infrared spectroscopy

(FTIR), as shown in Fig. S2. The peak at 3443 cm^{-1} implies the existence of residual hydroxyl groups, and the signal at 579 cm^{-1} is related to the stretching vibration of Fe-O in the two spectra. Compared with pure Fe_3O_4 spheres, the new peaks at 2918 cm^{-1} and 2846 cm^{-1} in the spectrum of FMAs are ascribed to the C-H stretching modes and the peaks at 1620 and 1450 cm^{-1} are attributed to -COOH vibrations, respectively. Besides, a series of peaks appeared at 1039 and 804 cm^{-1} are attributed to the stretching vibrations of a Si-O-Si stretching and Si-O bending in silane compound, respectively. The results showed the existence of carbon compound and C18TMS in the FMAs. Therefore, the carbon and silicon materials in the FMAs contain many hydrophobic groups and functional groups which could supply active sites in the adsorption process.^{10, 15}

TG-DTA measurement was employed to determine the amount of organic carbon present in the magnetic particles. Fig. S3 illustrates the results of the TG-DTA analysis of the Fe_3O_4 and FMAs, for which three-step weight loss occurs in the temperature region of $100\text{-}800\text{ }^\circ\text{C}$. The initial weight loss up to $150\text{ }^\circ\text{C}$ from the magnetic particles was probably due to loss of moisture, while the weight loss at higher temperature ($150\text{-}550\text{ }^\circ\text{C}$) could be mainly attributed to the evaporation and subsequent decomposition of the carbon compound. The last stage from $600\text{ }^\circ\text{C}$ to $700\text{ }^\circ\text{C}$ might be due to the continuous decomposition of the residue crystalline carbon and/ or silicon. There is no distinct weight loss when the temperature is higher than $700\text{ }^\circ\text{C}$, implying that only iron oxide or silicon compound is present in the temperature range of $700\text{-}800\text{ }^\circ\text{C}$. Finally, the organic carbon content of the solid Fe_3O_4 and FMAS is measured to be around $11.15\text{ wt}\%$ and

14.23 wt%.^{16, 17}

The morphology of the FMAs was observed, as typically shown in Fig. 1. The TEM images (Fig. 1a,b) shows that the FMAs consists of well-dispersed flower-like 3D submicron structures with a diameter varying from 130 to 160 nm, which different from the morphology of original Fe₃O₄ submicron spheres (Fig. S4). The detailed morphology of the flower-like structures is further shown in the high-magnification HAADF-STEM image (Fig. 1c), which reveals that the flower-like submicron spheres consist of entire structures of the architectures. It is clear that the FMAs are built from several dozen smooth surfaces of nanosheets with thickness about 5 nm. These nanopetals are further curled and intercrossed with each other. The STEM and TEM demonstrate that the morphology of FMAS is similar to that of other flower-like Fe₃O₄, however, the FMAs had a larger void space and a smaller diameter than those flower-like Fe₃O₄.^{6,9,11,18-20} Moreover, it is interesting to observe that many crystals distributed on the surface of the FMAs after adsorption of the Pb²⁺. It was probable that heavy metals existed either as adsorbed ions on the FMAs or as insoluble PbO and hydroxide precipitates.^{21, 22}

In addition, the porosity of the FMAs and the solid Fe₃O₄ was also confirmed by measurement of nitrogen adsorption-desorption isotherms (Fig. S5) and the BET surface area. The results indicated that the BET surface areas are 71.63 m²/g for FMAs, which is much higher than the values for Fe₃O₄ submicron particles (28.17 m²/g). Additionally, the Barrett-Joyner-Halenda (BJH) calculations for the pore size distribution (Table. 1) revealed that the pore size for the sample FMAs was centered at approximately 11.44 nm.

Such structure is favorable for application in water treatment, photocatalysis, drug delivery, enzyme immobilization, low density structure materials and so on.

The chemical elemental compositions of the FMAs were further studied by HAADF-STEM and EDX elemental mapping analysis. EDX measurements have revealed that there are Fe, C, Si and O elements in the products, except for Cu and a part of C element which comes from the carbon-coated copper grid, as shown in the inset of Fig. 2. The EDX results demonstrate that the FMAs contain carbon and oxygen-rich functional groups, which is in good agreement with the results of FTIR spectra. The chemical distribution of the FMAs was studied using HAADF-STEM and EDX elemental mapping. Figure 2a shows a representative HAADF-STEM image of an individual sphere. Figure 2b-f displays the corresponding EDX mappings of carbon ($K\alpha$, 0.28 keV), iron ($K\alpha$, 0.71 keV), iron ($L\alpha$, 6.4 keV), silicon ($K\alpha$, 1.74 keV) and oxygen ($K\alpha$, 0.52 keV) elements, respectively. It is seen that the elements C, Fe, Si and O, as detected by K-shell X-ray or L-shell X-ray, are evenly distributed throughout the whole FMAs. Such a carbonaceous and silicon material, uniformly distributed on the surface of the FMAS, would serve as active sites for the adsorption.

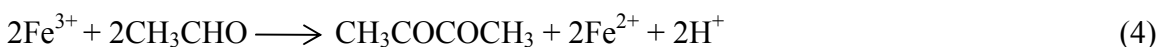
Magnetic property is the basic performance for magnetic particles, which is a key factor in deciding its future application. Hence, the magnetization curves of the Fe_3O_4 and FMAs are measured at room temperature. Fig. 3 and its inset show the corresponding magnetization curve with a hysteresis loop, indicating the typical ferromagnetic behavior in good agreement with the previously reported results.²³ The saturated magnetization

values of the Fe_3O_4 and FMAs are 88.91 emu/g and 44.41 emu/g, respectively. For the FMAs, the decrease in the value of M_s could be attributed to the reduced amount of Fe_3O_4 , which could be explained by the TG analysis that the mass ratio of the Fe_3O_4 in Fe_3O_4 particles is higher than that in FMAs. Anyway, these magnetic adsorbent could be separated from the reaction medium rapidly and easily in an external magnetic field. These results are the same with the previous report for the microstructural flower-like magnetic adsorbent.^{6, 11, 19, 20} Therefore, the functionalized flower-like magnetic adsorbent we prepared here showed narrow size distributions, excellent 3D hierarchical submicron structure, high specific surface area and large saturation magnetization.

According to the discussion above, we also studied the evolution of morphology during different reaction times. The SEM images of the resultant products are shown in Fig. S6. When the solvothermal reaction is 6 hour, a large amount of disorganized nanoplatelets are easily obtained, as shown in Fig. S6a. With an increase of the reaction time, more and more nanoplatelets along the oriented direction are formed with continuously increasing size (Fig. S6b). Subsequently, more and more nanoplatelets curve, intersect and overlap with one another, forming a multilayer and network structure (Fig. S6c). Consequently, the hierarchical flower-like submicron structures are formed until the final size is attained (Fig. S6d). However, by further prolonging the reaction time to sixteen hours, the samples were totally composed of numerous submicron particles and the surface of the submicron particles was very smooth. From this point, the reaction time is the crucial controlling factor in the formation of hierarchical flower-like

submicron structures. The corresponding schematic illustration for formation of the flower-like products is shown in Scheme 1.

As previous reported, the self-assembly of functionalized flower-like morphology may be caused by many forces, such as electrostatic and dipolar fields associated with the aggregate, hydrophobic interactions, hydrogen bonds, crystalface attraction, and van de Waals forces.²⁴ Based on the above previous reported, the functionalized flower-like adsorbents could have been formed involves three different stages: nucleation, growth and self-assembly, and Ostwald ripening.^{25, 26} It is usually supposed that EG acts as a high-boiling-point solvent and a reducing agent in the hydrothermal process, whereas sodium acetate provides a basic medium. The possible chemical reactions in this system are proposed as follows.^{27, 28}



First, a portion of Fe^{3+} ions, released from dissolving $\text{FeCl}_3 \cdot 6\text{H}_2\text{O}$, which were subsequently reduced by EG and converted into Fe^{2+} ions [reactions (3) and (4)]. At the same time, dissolved NH_4Ac in the solution would hydrolyze and release OH^- ions and NH_3 in the solution [reactions (5) and (6)]. The Fe_3O_4 formed by reaction of Fe^{3+} , Fe^{2+} and OH^- ions [reaction (7)].

In the following process, more ammonia gradually generates much more NH_3 to produce a lot of bubbles, which is favorable to form porous structured materials and also enhance the reducing ability of EG.^{27, 29} Then the concentration of Fe_3O_4 in the solution would be saturated, and hence Fe_3O_4 crystal nuclei are formed in the solution. The EDTA-2Na in the precursor solution can be hydrolyzed in the solution, and thus release EDTA anions, selective adsorption of EDTA anions on Fe_3O_4 crystal planes can alter its surface termination and atomic arrangement, which may have a great effect on the anisotropic growth process.⁸ Absence of TEOS and C18-TMS, the nuclei would subsequently grow into particles, as shown in S7. Thus, an appropriate amount of TEOS and C18-TMS is vital for the formation of functionalized flower-like submicron structure.³⁰

3.2 Water-treatment application

Considerable attention has been paid to environmental problems involving water treatment in recent years. Porous materials with high specific surface area are usually employed for wastewater treatment because of their capability to adsorb a large quantity of pollutants, and/or high-efficiency in degrading the unwanted species.¹⁸ The as-prepared FMAs, which have flower-like submicron structure, the high surface area, rich functional groups (-COOH, -OH and hydrophobic group) and magnetic properties, could be a good absorbent for the adsorption of dyes and heavy metal ions. Herein, we take two types of typical pollutants, dye (methylene blue (MB) and malachite green (MG)) and toxic heavy metal ions (Cr(VI) and Pb(II)) to be chosen as the model organic and

inorganic pollutant in water environment. UV-Vis absorption spectroscopy measurements were performed to determine the concentration of pollutants before and after treatment. For comparison, the adsorption ability of pure Fe_3O_4 was also studied.

3.2.1. Adsorption kinetics.

The dynamics of the adsorption process in terms of the order and the rate constant can be evaluated using the kinetic adsorption data. Fig. 4 shows the UV-Vis spectra of dye solutions before and after adsorption of the FMAS and Fe_3O_4 . From the Fig. 4a, b and the inset photograph, after being treated with FMAs adsorbent, only nearly colourless solution was remained within 6 minutes. The optical absorption peak, corresponding to MB and MG, almost disappears within 6 minutes. By contrast, the solid Fe_3O_4 submicron particles can adsorb hardly both for MB and MG molecules as shown in Fig. 4c, d. The color and the optical absorbance spectra of the MB and MG solution changed rarely within initial 5 minutes. Obviously, the FMAs can adsorb MB and MG far more effectively and quickly than the solid Fe_3O_4 submicron particles, which is very important to save cost in the real water-treatment process. It is believed that the novel and high efficient material can be extended to remove other environment pollutants in wastewater.

To further verify the advantage of FMAS in water treatment, we evaluate the adsorption capabilities for toxic heavy metal ions at room temperature. The adsorption kinetic curves of Cr(VI) (pH=3.0) and Pb(II) (pH =5.0) on FMAS and Fe_3O_4 with an initial concentration of 100 mg/L are shown in Fig. 5. It was observed that the maximum capacity of adsorption of Cr(VI) and Pb(II) were 26.4 and 31.5 mg/g for FMAS, 18.7 and

6.6 mg/g for Fe_3O_4 , respectively. Therefore, it can be seen that the as-obtained FMAS possess remarkably better removal capacity than the solid Fe_3O_4 submicron particles. According to these data, initial adsorption of Cr (VI) and Pb (II) were rapid on the FMAS and Fe_3O_4 within the first 1 hour. The adsorption sites on the adsorbents were quickly covered by Cr(VI) and Pb(II), and the adsorption rate became dependent on the rate at which the metal ions were transported from the bulk liquid phase to the actual adsorption sites. Thus the contact time of 15 h was used in the following sections to ensure the adsorption equilibrium of Cr(VI) and Pb(II) onto the FMAS and Fe_3O_4 submicron particles. It was found that FMAS showed similar removal ability for Cr (VI) and Pb (II) to the effective activated carbon from most of the raw materials (Hevea Brasilinesissawdust activated carbon, q_{max} , 44.05 mg/g for Cr(VI), pine cone activated carbon, q_{max} , 27.53 mg/g for Pb (II)).^{31,32} The kinetics of removal of Pb (II) and Cr (VI) are also tested with pseudo first-order, second-order and Elovich kinetic models to examine the rate controlling mechanism of the adsorption process (Fig. S8 and table S1), among which the second order kinetic model fit the experimental data well. Overall, these observations suggest that the process controlling the rate may be a chemical sorption.³³

3.2.2. Adsorption isotherms.

A better understanding is achieved by adsorption isotherm that reveals the distribution of adsorbed molecules between the liquid phase and solid phase. Also, the adsorption isotherm gives an idea of the adsorption capacity of the adsorbent.³⁴ The

adsorption isotherms of MB, MG, Cr(VI) and Pb(II) on the FMAs and Fe₃O₄ are shown in Fig. 6. As shown in Fig. 6a, the FMAs had better adsorption capacity for MB and MG than the solid Fe₃O₄ submicron particles. The increasing initial MB or MG concentration resulted in an increase of MB or MG on the FMAs. The saturated adsorption amount is much higher, for the FMAs (~ 40 mg/g) than that for the Fe₃O₄ submicron particles (~ 4 mg/g), showing significantly enhanced adsorption performance. Fig. 6b depicts the adsorption isotherms of Pb (II) and Cr (VI) ions on the FMAs and Fe₃O₄. The adsorption capacity of Pb (II) and Cr (VI) by the magnetic absorbents increased rapidly with increase in the heavy metal ions concentration in the range of 10-100 mg/L, while increased slowly as the ion concentration was higher than 100 mg/L. The maximum adsorption capacities for Pb (II) and Cr (VI) ions in the concentration range studied are 72.1 and 76.8 mg/g for FMAS, 43.0 and 41.9 mg/g for Fe₃O₄, respectively. These adsorption capacities of the FMAS are higher than those of previously reported materials.^{12,35} At the concentration below 20 mg/L, Cr (VI) in the solution would interact with the binding sites and thus facilitated more than 90% adsorption for the FMAs, which is higher than that for the solid Fe₃O₄ (40%). This result shows that the FMAs can treat wastewater with low concentrations of Cr (VI).

Further investigate the mechanism of adsorption for both samples, the Langmuir and Freundlich isotherm models³⁶ are applied to analyze the experimental data and applied for the adsorption of the pollutants on the absorbents (Fig. S9). The Langmuir model is expressed as:

$$q_e = \frac{bq_{\max}C_e}{1+bC_e} \quad (8)$$

The Freundlich isotherm model can be expressed by the following equation:

$$q_e = kC_e^{1/n} \quad (9)$$

Where C_e is the initial and equilibrated concentrations; q_e is the amount adsorbed on unit mass of the adsorbent (mg/g); q_{\max} is the quantity of adsorbate required to form a single monolayer on unit mass of adsorbent (mg/g); and b is the Langmuir adsorption constant (L/mg) which describes the affinity in the adsorption process. The Freundlich constant k is correlated to the relative adsorption capacity of the adsorbent (mg/g), and $1/n$ is the adsorption intensity.

Table S2 summarizes the Langmuir and Freundlich constants and the calculated coefficients. It can be found that the adsorption isotherm fits the Langmuir model better than Freundlich model for the adsorption of MG and MB on the FMAS. The results highlight the homogeneous nature of samples surface and the formation of monolayer coverage of dye molecules on the FMAS. Hence, larger number of vacant surface sites is available for adsorption of dye with higher specific surface area.³⁷ The maximum adsorption capacity of the FMAS was found to be 40.82 mg/g for MG and 44.44 mg/g for MB. The high MB adsorption capacity may be due to its high surface area and the unusual tertiary structure. In addition to the structurally enhanced adsorption, the surface functional groups should also be responsible for the enhanced adsorption capacity. Due to the existence of -COOH, the surface of the FMAS should be negatively charged.²⁸ The MB and MG are organic positively charged molecules, which contains many groups

(N=C or S=C).³⁸ Therefore, the FMAs composites can adsorb the positively charged MB and MG molecules by electrostatic interaction. Meanwhile, the adsorption of dye molecules onto FMAs surfaces is related to the hydrophobic groups (long (C18) chains) on the surface of the adsorbent. These hydrophobic groups on the adsorbent's surface would resist integrating water with the adsorbent's surface. Due to their surface hydrophobic groups, the organic dye molecules are more favorable for approaching the adsorbent's surface.³⁹ Therefore, the extraordinary fast adsorption rate may be attributed to two factors: (i) the electrostatic attraction between the negatively charged surface of the FMAs and the cationic MB and MG; (ii) the unusual tertiary structure and high BET surface area of the FMAs,^{1,37} (iii) the hydrophobic interaction between the dye and the hydrophobic space of the FMAs. Also because of such, the poor removal performance of the solid Fe₃O₄ for MB and MG may be due to their low surface area and weak electrostatic and hydrophobic interactions of the materials.

Furthermore, the parameters reveal that the adsorption of Pb (II) and Cr (VI) ions on the FMAs and the solid Fe₃O₄ agree well with the Freundlich mode than the Langmuir, which suggests the adsorption is heterogeneous. This fact can be justified both physical and chemical adsorption of the magnetic adsorbent were exist at the same time. On the basis of the FTIR spectra (Fig. S2), the FMAs had a large number of hydroxyl and carboxyl groups, which can interact with Pb (II) and Cr (VI) ions through complexation, ion exchange, electrostatic attraction, as well as availability of active surface sites.^{40,41} Figure S10 displays the corresponding EDX mappings results of the FMAs after

adsorption of Pb (II). It is seen that the element Pb are evenly distributed throughout the whole FMAs. In addition, physical adsorption may be responsible for the interaction between the FMAs and heavy-metal ions due to the high surface area and porous structure of the FMAs. Whereas, the surfaces of the solid Fe_3O_4 contains a little amount of oxygen groups, so relatively few heavy metal ions are likely adsorbed on the solid Fe_3O_4 based on the combination of electrostatic interactions between charged oxides and ions, and ion exchange in the aqueous solution.^{8,42} Moreover, the magnetic separation technology provides a rapid and effective technology for separating the magnetic adsorbents from aqueous phase.

3.2.3. Simultaneous adsorption of Pb(II) and MG.

Various pollutants such as dye stuffs, suspended solids, other soluble organic substances, and heavy metals are generally present in the textile and dyeing industry wastewaters, and these coexisting pollutants may interfere with each other through competitive binding or complexation during the removal process.⁴³ Therefore, understanding of multicomponent interaction with magnetic adsorbent would be very helpful for its use in wastewater treatment. In the study, the simultaneous Pb (II) and MG adsorption experiments were conducted. As shown in Fig. 7, it was found that the FMAs showed much better adsorption ability for Pb (II) and MG than that of the solid Fe_3O_4 . The Pb (II) adsorption onto the FMAs and the solid Fe_3O_4 in the presence of MG is higher than that in the absence of MG. These results may be due to the fact that MG in the solution can be adsorbed by the surfaces of the magnetic adsorbents to form the

MG-adsorbent, resulting in more organic functional groups presenting in the magnetic adsorbents to enhance the Pb (II) adsorption.³⁹ Whereas, the adsorption capacities of FMAs and the solid Fe₃O₄ for MG in the presence of Pb (II) are lower than those in the absence of Pb (II). One possible reason is that there are a number of adsorptive sites (such as -COOH) for Pb (II) binding, leading to the decrease of MG adsorption. Therefore, the FMAS is a suitable low-cost adsorbent that is economically attractive and at the same time present similar or even better characteristics than the conventional adsorbents materials.⁴⁴⁻⁴⁶

4. Conclusion

In summary, a facile one-pot, and environment-friendly solvothermal method was developed for the synthesis of functionalized flower-like magnetic submicron structures with large surface area using iron(III) chloride hexahydrate as precursor, ethylene glycol as reducing agent, ammonium acetate and EDTA-2Na as electrostatic stabilization agent. The EDTA-2Na, TEOS and C18-TMS should be responsible for the self-assembly of the nanoplates and final flower-like morphology. Due to the high surface area and rich surface functional groups, the FMAs exhibit an enhanced adsorption performance to dyes and heavy metal ions in the binary system, compared with that of the solid Fe₃O₄ submicron particles. The as-prepared FMAs showed an excellent ability to remove heavy metal ions and dye in water treatment and are expected to be useful in many other applications.

Acknowledgment

The authors thank the financial supports from the National Natural Science Foundation of China (No.21074049), the National Basic Science Foundation for undergraduate students (J1103307), the Opening Foundation of State Key Laboratory of High Performance Civil Engineering Materials (2011CEM006), and the Fundamental Research Funds for the Central Universities (lzujbky-2012-75).

References

- [1] L. Sun, C. G. Tian, L. Wang, J. L. Zou, G. Mu and H. G. Fu, *J. Mater. Chem.*, 2011, **21**, 7232-7239.
- [2] O. H. Ramirez and S. M. Holmes, *J. Mater. Chem.*, 2008, **18**, 2751-2761.
- [3] S. Singh, K. C. Barick and D. Bahadur, *J. Mater. Chem. A*, 2013, **1**, 3325-3333.
- [4] Y. Q. Chen, L. B. Chen, H. Bai and L. Li, *J. Mater. Chem. A*, 2013, **1**, 1992-2001.
- [5] Z. B. Gan, A. W. Zhao, Q. Gao, M. F. Zhang, D. P. Wang, H. Y. Guo, W. Y. Tao, D. Li, E. H. Liu and R. R. Mao, *RSC Adv.*, 2012, **2**, 8681-8688.
- [6] X. Y. Li, Z. J. Si, Y. Q. Lei, X. N. Li, J. K. Tang, S. Y. Song and H. J. Zhang, *CrystEngComm*, 2011, **13**, 642-648.
- [7] A. M. Cao, J. S. Hu, H. P. Liang and L. J. Wan, *Angew. Chem.-Int. Edit.*, 2005, **44**, 4391-4395.
- [8] X. B. Wang, W. P. Cai, G. Z. Wang, Z. K. Wu and H. J. Zhao, *CrystEngComm*, 2013, **15**, 2956-2965.
- [9] L. Han and Y. Wei, *Mater. Lett.*, 2012, **70**, 1-3.
- [10] L. X. Wang, J. C. Li, Q. Jiang and L. J. Zhao, *Dalton Trans.*, 2012, **41**, 4544-4551.
- [11] L. X. Wang, J. C. Li, Z. T. Wang, L. J. Zhao and Q. Jiang, *Dalton Trans.*, 2013, **42**, 2572-2579.
- [12] L. S. Zhong, J. S. Hu, H. P. Liang, A. M. Cao, W. G. Song and L. J. Wan, *Adv. Mater.*, 2006, **18**, 2426-2431.

- [13] Z. H. Ai, K. J. Deng, Q. F. Wan, L. Z. Zhang and S. C. Lee, *J. Phys. Chem. C*, 2010, **114**, 6237-6242.
- [14] H. Deng, X. L. Li, Q. Peng, X. Wang, J. P. Chen, Y. D. Li, *Angew. Chem. Int. Ed.*, 2005, **44**, 2782-2785.
- [15] H. X. Wu, G. Liu, S. J. Zhang, J. L. Shi, L. X. Zhang, Y. Chen, F. Chen and H. R. Chen, *J. Mater. Chem.*, 2011, **21**, 3037-3045.
- [16] S. K. Li, F. Z. Huang, Y. Wang, Y. H. Shen, L. G. Qiu, A. J. Xie and S. J. Xu, *J. Mater. Chem.*, 2011, **21**, 7459-7466.
- [17] X. Liu, Y. F. Li, W. W. Zhu and P. F. Fu, *CrystEngComm*, 2013, **15**, 4937-4947.
- [18] B. Wang, H. B. Wu, L. Yu, R. Xu, T. T. Lim and X. Wen, *Adv. Mater.*, 2012, **24**, 1111-1116.
- [19] Q. Gao, A. W. Zhao, Z. B. Gan, W. Y. Tao, D. Li, M. F. Zhang, H. Y. Guo, D. P. Wang, H. H. Sun, R. R. Mao and E. H. Liu, *CrystEngComm*, 2012, **14**, 4834-4842.
- [20] L. H. Han, Y. C. Chen and Y. Wei, *CrystEngComm*, 2012, **14**, 4692-4698.
- [21] X. D. Li, C. S. Poon, H. Sun, I. M. C. Lo and D. W. Kirk, *J. Hazard. Mater.*, 2001, **82**, 215-230.
- [22] M. I. Litter, *Appl. Catal. B- Environ.*, 1999, **23(2)**, 89-114.
- [23] F. Cao, W. Hu, L. Zhou, W. D. Shi, S. Y. Song, Y. Q. Lei, S. Wang and H. J. Zhang, *Dalton Trans.*, 2009, 9246-9252.
- [24] X. Y. Li, M. R. Gao, S. R. Zhang, J. Jiang, Y. R. Zheng, D. Q. Tao and S. H. Yu, *J. Mater. Chem.*, 2011, **21**, 16888-16892.
- [25] J. M. Ma, T. H. Wang, X. C. Duan, J. B. Lian, Z. F. Liu and W. J. Zheng, *Nanoscale*, 2011, **3**, 4372-4375.

- [26] F. P. Dong, W. P. Guo, C. S. Ha, *J. Nanopart Res.*, 2012, **14**, 1-8.
- [27] X. H. Lin, G. B. Ji, Y. S. Liu, Q. H. Huang, Z. H. Yang and Y. W. Du, *CrystEngComm*, 2012, **14**, 8658-8663.
- [28] R. Demir-Cakan, N. Baccile, M. Antonietti and M. M. Titirici, *Chem. Mater.*, 2009, **21**, 484-490.
- [29] Q. Peng, Y. J. Dong and Y. D. Li, *Angew. Chem. Int. Ed.*, 2003, **42**, 3027-3030.
- [30] M. Kim, K. Sohn, J. Kim and T. Hyeon, *Chem. Commun.*, 2003, 652-653.
- [31] Momčilović M, Purenović M, Bojić A, Zarubica A and Randelović M, *Desalination*, 2011, **276(1)**, 53-59.
- [32] T. Karthikeyan, S. Rajgopal and Lima Rose Miranda, *J. Hazard. Mater.*, 2005, **124(1)**, 192-199.
- [33] Y. Zhang, Y. F. Li, X. L. Li, L. Q. Yang, X. Bai, Z. F. Ye, L. C. Zhou and L. Y. Wang, *J. Hazard. Mater.* 2010, **181**, 898-907.
- [34] W. Fan, W. Gao, C. Zhang, W. W. Tjiu, J. Pan and T. X. Liu, *J. Mater. Chem.*, 2012, **22**, 25108-25115.
- [35] L. Q. Ji, L. C. Zhou, X. Bai, Y. M. Shao, G. H. Zhao, Y. Z. Qu, C. Wang and Y. F. Li, *J. Mater. Chem.*, 2012, **22**, 15853-15862.
- [36] X. Yang, C. L. Chen, J. X. Li, G. X. Zhao, X. M. Ren and X. K. Wang, *RSC Adv.*, 2012, **2**, 8821-8826.
- [37] D. P. Zhang, C. H. Lu, Y. R. Ni, Z. Z. Xu, W. B. Zhang, *CrystEngComm*, 2013, **15**, 4755-4764.
- [38] Z. H. Sun, L. F. Wang, P. P. Liu, S. C. Wang, B. Sun, D. Z. Jiang and F. S. Xiao, *Adv. Mater.*, 2006, **18**, 1968-1971.
- [39] J. P. Chen, S. Wu, *J. Colloid. Interf. Sci.*, 2004, **280**, 334-342.

- [40] L. Q. Yang, Y. F. Li, X. L. Jin, Z. F. Ye, X. J. Ma, L. Y. Wang, Y. P. Liu, *Chem. Eng. J.*, 2011, **168**, 115-124.
- [41] H. Wang, Y. F. Yu, Q. W. Chen and K. Cheng, *Dalton Trans.*, 2011, **40**, 559-563.
- [42] N. Mao, L. Q. Yang, G. H. Zhao, X. L. Li, Y. F. Li, *Chem. Eng. J.*, 2012, **200-202**, 480-490.
- [43] Y. J. Wu, L. J. Zhang, C. L. Gao, J. Y. Ma, X. H. Ma and R. P. Han, *J. Chem. Eng.*, 2009, **54**, 3229-3234.
- [44] Y. H. Li, Z. Di, J. Ding, D. Wu, Z. Luan and Y. Zhu, *Water Res.*, 2005, **39**, 605-609.
- [45] T. Santhi, S. Manonmani and T. Smitha, *J. Hazard. Mater.*, 2010, **179(1)**, 178-186.
- [46] L. Y. Wang, L. Q. Yang, Y. F. Li, Y. Zhang, X. J. M and Z. F. Ye, *Chem. Eng. J.* 2010, **163(3)**, 364-372.

Table 1 Textural properties of Fe₃O₄ and FMAs adsorbents

adsorbents	Surface area (m ² /g)	Total pore volume (cm ³ /g)	Average pore diameter (nm)
Fe ₃ O ₄	28.17	0.083	-
FMAs	71.63	0.205	11.44

Captions of Figures

Fig. 1 (a) representative TEM image of the FMAs; (b) high-magnification TEM image of the FMAs; (c) high-magnification STEM image of the FMAs; (d) high-magnification STEM image of the FMAs after adsorption of the Pb(II).

Fig. 2 Elemental mappings of the FMAs: (a) representative HAADF-STEM image of FMAs; inset shows the EDX spectrum acquired from the FMAs; (b) carbon mapping; (c) oxygen mapping; (d) silicon mapping; (e) iron mapping ($K\alpha$); and (f) iron mapping ($L\alpha$).

Fig. 3 Magnetization hysteresis loops of the Fe_3O_4 spheres and FMAs.

Fig. 4 The UV-Vis absorbance spectra of the 8 ml solution with initial MB or MG (pH=6.5) concentration 25 mg/ L and 16 mg magnetic adsorbents after adsorption for different times. The inset is photos of the MB or MG solutions after adsorption for the corresponding time, and separation of the composites from solution by a magnet. (a) UV-Vis spectra of MB solution adsorbed with the FMAs. (b) UV-Vis spectra of MG solution adsorbed with the FMAs. (c) UV-Vis spectra of MB solution adsorbed with the Fe_3O_4 solid spheres. (d) UV-Vis spectra of MG solution adsorbed with the Fe_3O_4 spheres.

Fig. 5 Adsorption rate of the Pb(II) and Cr(VI) on the Fe_3O_4 spheres and FMAs.

Fig. 6 The adsorption isotherms of (a) MB, MG and (b) Cr(VI), Pb(II) on the FMAs and Fe_3O_4 spheres.

Fig. 7 The effect of different concentrations of Pb(II) and MG in binary mixtures.

Fig. 1

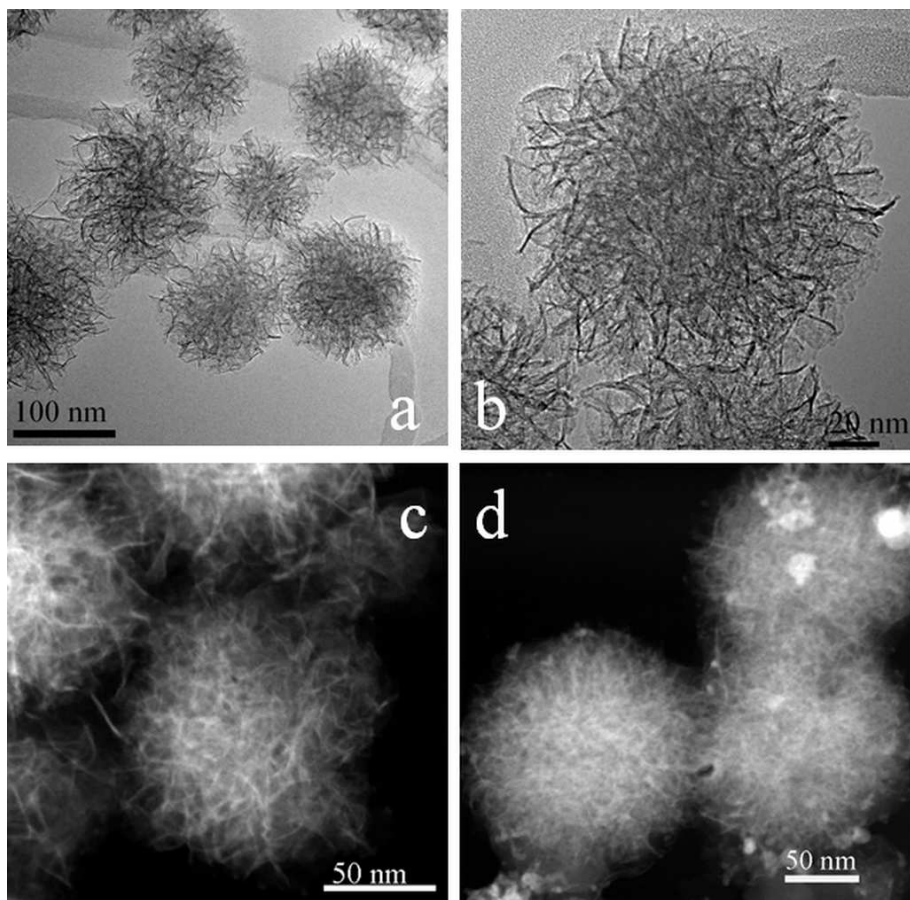


Fig. 2

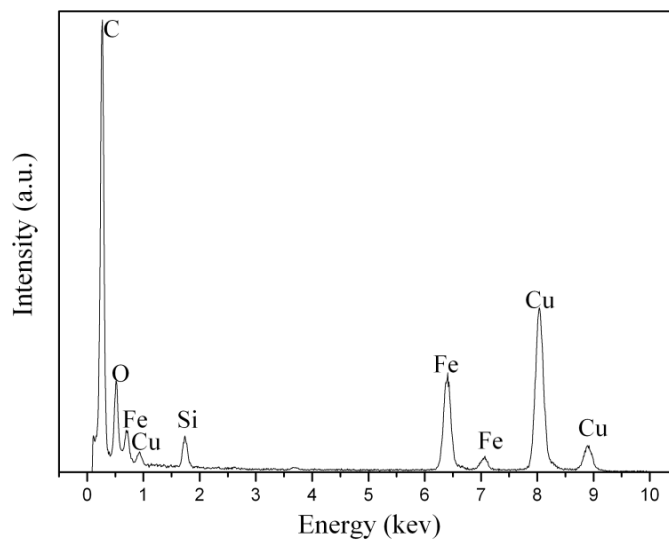
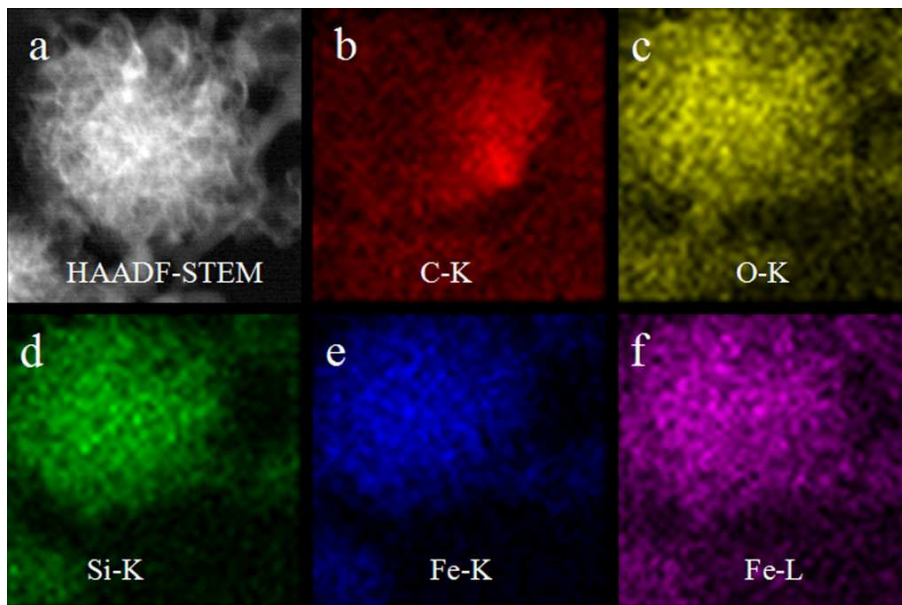


Fig. 3

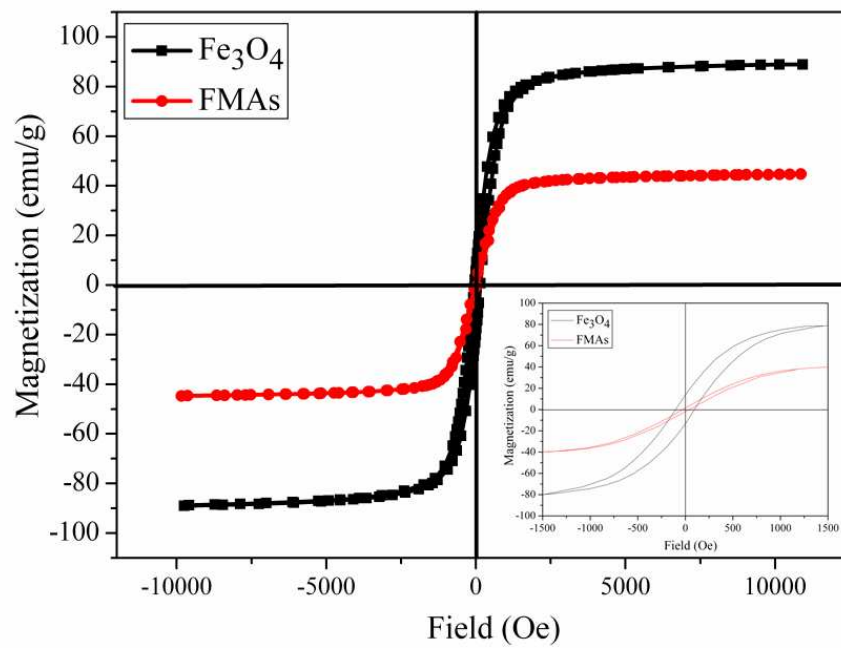


Fig. 4

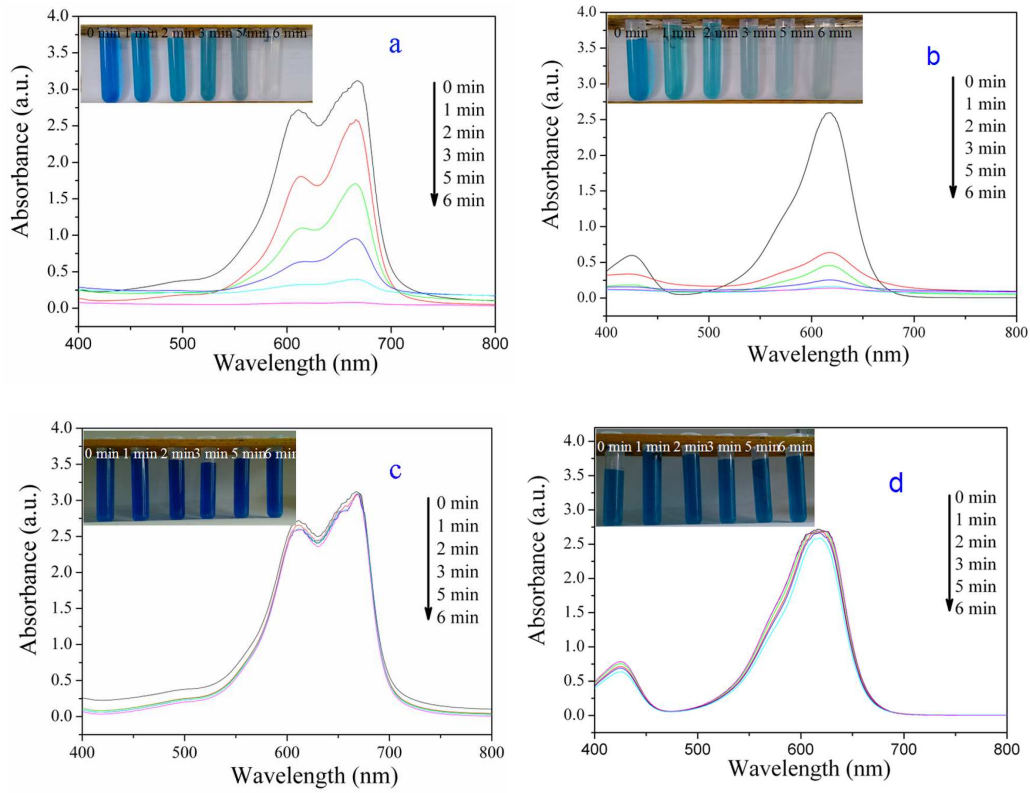


Fig. 5

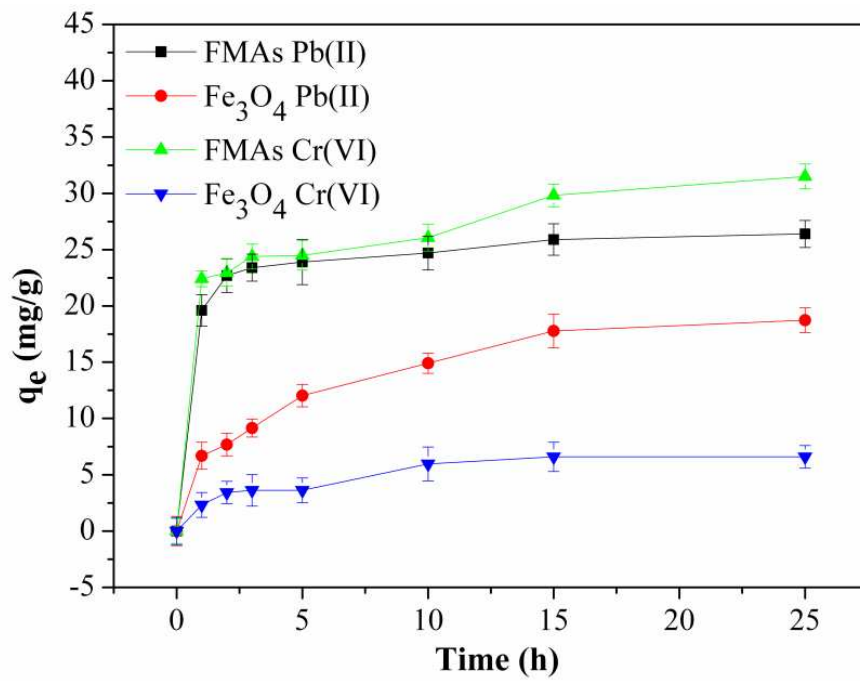


Fig. 6

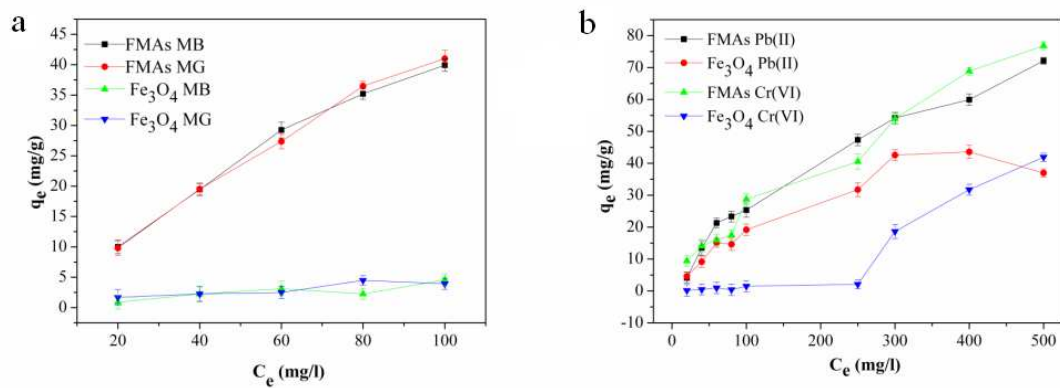
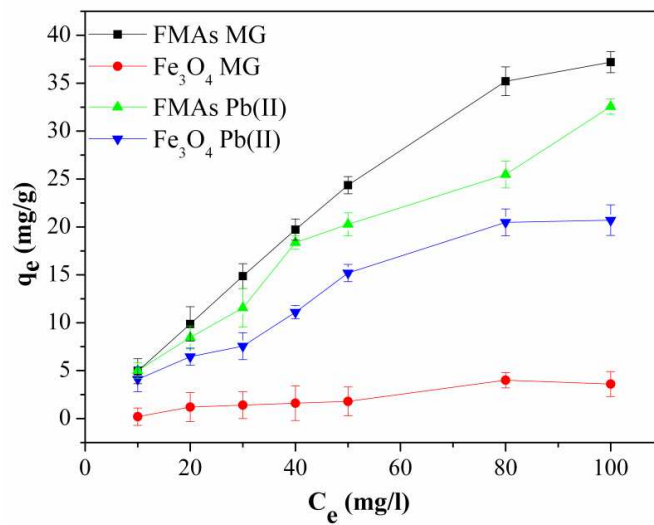
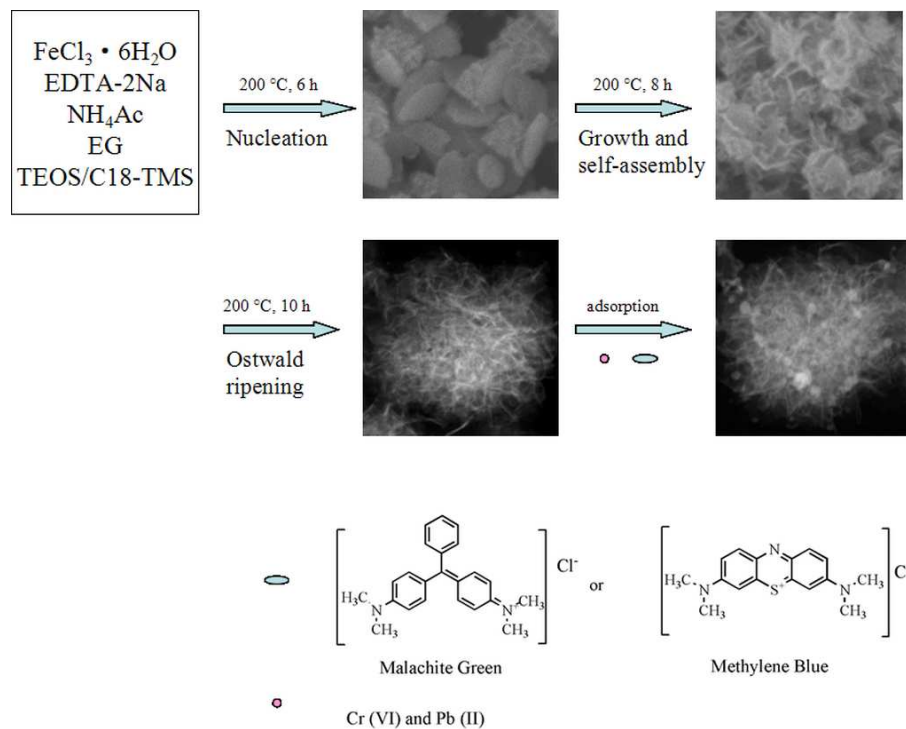


Fig. 7





Scheme 1 Schematic adsorption mechanisms on the FMAs.